

HYPERSPECTRAL IMAGING WITH LIQUID-CRYSTAL TUNABLE FILTER FOR TISSUES CHARACTERIZATION

Jong-Ha Lee^{1*} and Jeonghun Ku¹

¹ Keimyung University, School of Medicine, Daegu, South Korea
segeberg@kmu.ac.kr

ABSTRACT

We developed and characterized a new near-infrared hyperspectral imaging system. The system consists of a charged coupled device and liquid crystal tunable filter, which is continuously tunable in the near-infrared spectral range of 650-1100 nm with a mean bandwidth of 5 nm. Experiments are conducted to quantitatively determine normal tissues characterization. In the first experiment, hyperspectral images are acquired from normal lung tissue phantom and analyzed. The data shows obvious peak absorption intensity at four different near infrared wavelengths (760, 805, 905, and 970 nm). In the second experiment, the simulated malign lung tissue phantom is used to compare the spectrum between normal and malign tissues. The experimental result indicates that for different type of tissues, the absorption intensity of the spectrum integrated over near-infrared spectral region was considerably different in normal tissues and simulated malign tissues. This difference provides the basis for the detection and delineation of the malign tissue margins from the normal tissues.

KEYWORDS

Hyperspectral, Tissue, Imager, Non-Invasive Method, Near-Infrared

1. INTRODUCTION

Hyperspectral imaging system (HIS) is a novel method to generate a spectral characteristic map of region of interest (ROI) based on the chemical composition. Previously, HIS has been used in non-medical applications including satellite investigation to find minerals on the ground or to access the condition of agriculture fields. Recently, HIS has been applied to the investigation of pathological changes in living tissue of animal and human. It has proven that HIS can provide valuable information as to the health or disease of tissue that sometimes other modalities are unavailable. HIS is a remote sensing technology to create 2-dimensional image having spectral information in each pixel. This information can be interpreted as the gradient map of species. It means HIS is a method of imaging spectroscopy combining the chemical specificity of spectroscopy with spatial information of imaging. The general concept of hyperspectral imaging is shown clearly in Fig. 1.

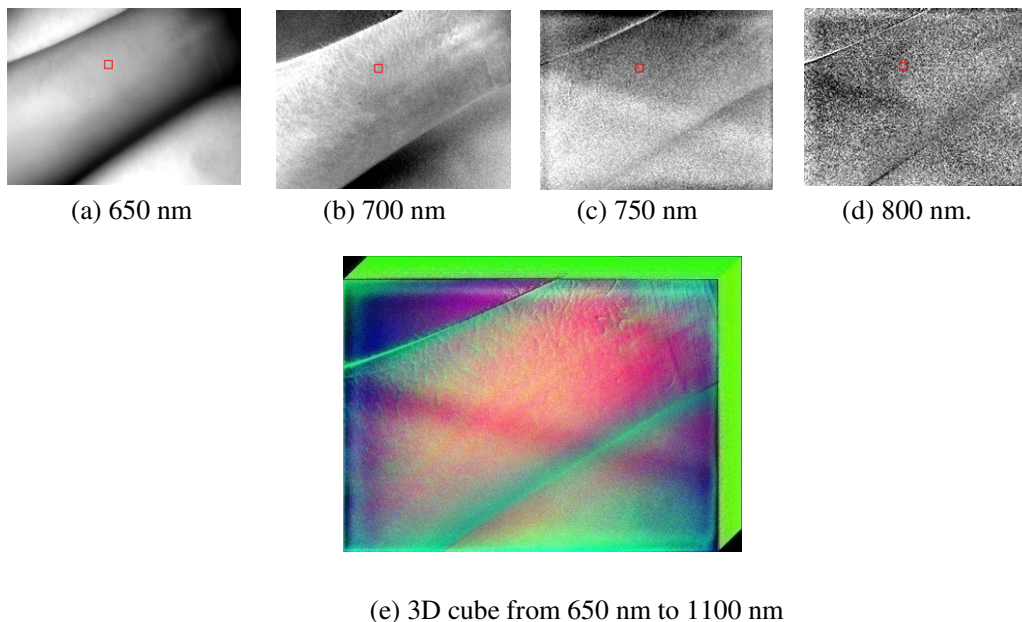


Figure 1. Near infrared hyperspectral imaging of human arm in the wavelength of (a) 650 nm (b) 700 nm (c) 750 nm (d) 800 nm. (e) 3D hyperspectral cube reconstruction using the image from 650 nm to 1100 nm with 5 nm interval.

Biological tissues have optical signatures that reflect their chemical characteristics. The primary compositions in human tissue are oxyhemoglobin (HbO₂) and deoxyhemoglobin (Hb). The Hb further breaks down into melanin, lipids and water (oxygenation). Total hemoglobin (HbT) indicates the combined quantities of HbO₂ and Hb. In near infrared (NIR) region, HbO₂ and Hb are major sensitive spectrum absorber. Since many diseases have specific effects on tissue oxygen and blood supply, tissue oxygenation and total hemoglobin concentration are major indicators of viability and tissue health. Thus in this paper, we mainly focus on the NIR region, particularly the short wavelength NIR of 650 to 1100 nm. By comparing the acquired spectrum absorption measurement in NIR region, information about type, location and relatively concentration of chemical decomposition about the tissue can be quantified. As far as we know, non-invasive, real time, local measurement of tissue oxygenation and total hemoglobin is still not commercially available. In this paper, we construct and characterize of HIS capable of detecting photons in the NIR wavelength region to characterize the tissue condition. HIS we propose here has several advantages compare to other modalities such as CT and MRI. It penetrated into biological tissue deeply without radiation exposure such as CT, thus functional imaging with non-invasive and non-radioactive in real time is available. In addition it is portable and low cost compared to MRI.

The object of this work is to design HIS and investigate the ability of detecting normal tissues and distinguishing normal tissues from malign tissues. HIS is integrated with charged coupled device (CCD) and liquid crystal tunable filter (LCTF) to automatically capturing the spectrum information. LCTF controller is tuned to scanning from 650 nm to 1100 nm bands with 5 nm steps. From the data, the absorption spectrum of HbO₂, Hb, lipids and water of normal and malign tissues are characterized and compared. The experimental study demonstrates the system capability of characterization of normal tissues and discriminate it from malign tissues by identifying key wavelengths. Identifying key wavelengths for tissue characteristic provides crucial in reducing the amount of data collected in subsequent specimen studies, thus allowing for rapid, optical, and clinical diagnosis.

2. EXPERIMENTAL SETUP

2.1. System Description

The portable hyperspectral tunable imaging system consists of 1.4 megapixel 12 bit digital imager (Qimaging Inc., Surrey, British Columbia), Liquid Crystal Tunable Filter (LCTF, Cambridge Research & Instrumentation Inc., Woburn, Massachusetts), and LCTF controller. The digital imager is a mono-cooled Charge Coupled Device (CCD) with $1392 (V) \times 1040 (H)$ spatial resolution with $6.45 \mu m (V) \times 6.45 \mu m (H)$ individual pixel size. LCTF is placed in front of the digital imager and filters bands in the short wavelength NIR range from 650 nm to 1100 nm. The filter is set to 5 nm full width at half maximum (FWHM). The FWHM is measured as the spectral separation between two points where the filter's transmission attains 50 % of the peak value. The LCTF controller synchronizes between digital imager and LCTF and switches the programmed sequential bands of filter. The tuning speed of the filter is between 50 ms to 150 ms.

All images were captured with 91 bands with center wavelengths separated by 5 nm. Data produced by HIS can be represented by a 3-D cube of image $I(x, y, \lambda_k)$, where (x, y) indicates the spatial coordinate of a pixel in the size, $x = 1, 2, \dots, 1,392$, $y = 1, 2, \dots, 1,040$, and λ_k denotes the wavelength of the k^{th} spectral band. Each value of $I(x, y, \lambda_k)$ is quantified by a grey scale level and has a minimum value of 0 and has a maximum value of $2^{12} = 4,096$. Individual 3-D cube of images are stored in a 12 bit binary format along a header file containing image parameter information. The data size of one image is approximately $1,392 \text{ pixels} \times 1,040 \text{ pixels} \times 91 \text{ bands} \times 12 \text{ bits} = 197 \text{ megabytes}$. LCTF tuning, image acquisition, and storage are managed by a software compile by C++. A high-end laptop computer (Apple MacPro 2.53 GHz, Cupertino, CA) manages the instrument control, spectral image acquisition and synchronization. Image visualization is performed using ENVI software environment (Ver. 4.5, ITT Visual information solutions, Boulder, CO). The total scanning of LCTF is about 23 seconds including data transferring to computer and image rendering to screen. Fig. 2. shows HIS system in detail. HIS consists of three part, computer to LCTF controller, LCTF controller to camera, and camera to computer. The synchronization of this system is performed in the computer. Fig. 3. represents HIS transmission characteristics. Total bands from 650 nm – 1100 nm perform the similar transmission characteristics.

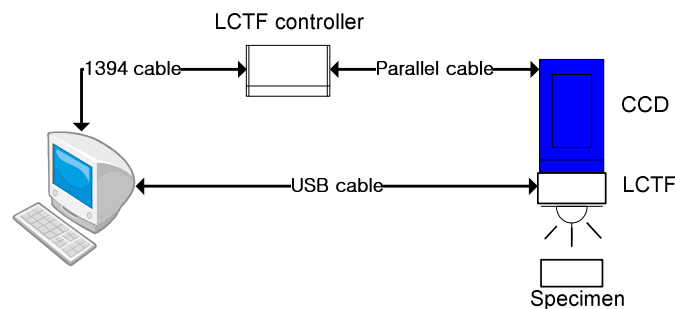


Figure. 2. Schematic diagram of the hyperspectral imaging system.

The connection consists of three parts. From computer to LCTF controller, 1394 cable is connected. From LCTF controller to camera, parallel cable is used. From camera to computer, USB cable is connected. The synchronization of this connection is handled in the computer.

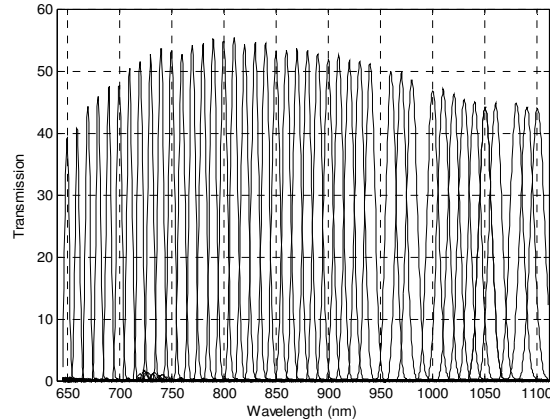


Figure. 3. Hyperspectral imaging system transmission characteristic at NIR 650 nm – 1100 nm. The transmission gives similar transmission characteristic.

2.2. Excitation Light Subsystem

To cover the short wavelength spectral range, two types of light sources are used for illumination. In the preliminary experiments, dual 500 W white quartz tungsten halogen lamps (QTH) range from 360 nm to 2500 nm was used. However, poor luminous efficiency (10 ~ 20 lm/W), non uniform illumination, and the overheating problem, it was not appropriate to use our purpose. To increase the luminous efficiency and prevent the overheating of the sample tissue, low working temperatures and high luminous efficiency Light Emitted Diode (LED) illuminator is considered with the following design. First a custom matching box with 99% reflection coating is machined such that its 10 mm diameter end hole fit into the nosepiece of fiber bundle. Inside a matching box, there is a LED array panel for illumination and a cooling fan to regulate the temperature of inside the box caused by LED array. The LED array panel consists of LR W5AP Osram Diamond Dragon LEDs. The luminous efficiency of this LED is 45 lm/W with 140 degree viewing angle. To make a same performance of 500 W QTH, paralleled 110 LEDs is integrated onto the single Printed Circuit Board (PCB). Since the illuminator needs to focus on the 10 mm diameter hole, the round shape of PCB with 30° is used. Regarding the light guide, an optical fiber bundle consists of Corning SMF-28e optical fibers with 8.2 μm core diameters are customized and 6.35 mm stainless steel houses an optical fiber bundle. The connector between a matching box and a nosepiece of an optical fiber bundle is sealed with aluminum tape to eliminate light leakage. The light is then transmitted through an optical fiber bundle towards a light reflector and illuminates a sample. The illumination angle is within 5° to minimize the shadows and directional scattering caused by the rough surface of the subjects. Fig. 4a and 4b indicates the proposed layout of QTH and LED array excitation light subsystem.

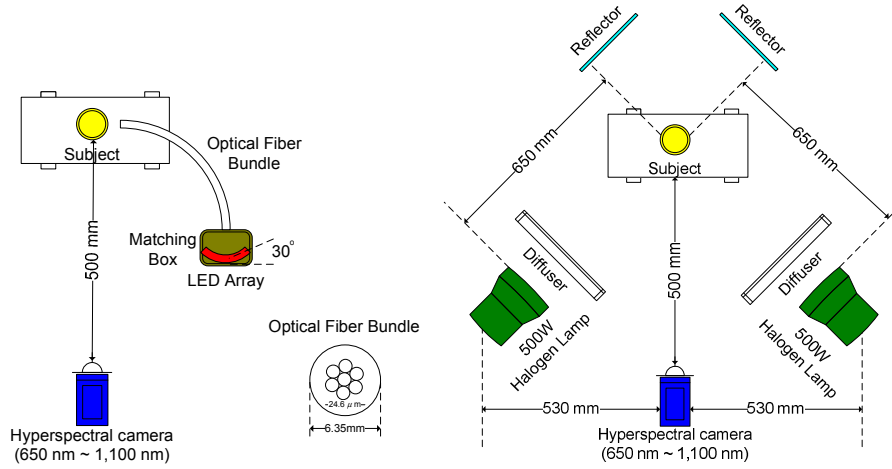


Fig. 4. (a) The layout of a hyperspectral imaging system with dual 500W Halogen Lamp Illuminator. (b) The layout of a hyperspectral imaging system with LED Array Illuminator

2.3. Optics Calibration

Since image intensity data from digital imager have unknown system offsets and gains and may vary over time, an image intensity converted to the reflectance data. According to [1], image intensity at spatial coordinate (x, y) at λ_k band can be modeled as

$$I(x, y, \lambda_k) = L(x, y, \lambda_k)S(x, y, \lambda_k)R(x, y, \lambda_k) + O(x, y, \lambda_k) \quad (1)$$

where $x = 1, 2, \dots, 1392$, $y = 1, 2, \dots, 1040$, and $k = 1, 2, \dots, 91$. $L(x, y, \lambda_k)$ refers to the illumination, $S(x, y, \lambda_k)$ refers to the system spectral response, $R(x, y, \lambda_k)$ refers to the reflectance of the viewed surface, and $O(x, y, \lambda_k)$ is the offset due to the stray of the light. To compensate unknown system offsets and gains, Spectralon diffuse reflectance standards SRS-99 for an approximately 99 % reflectance and SRS-02 for an approximately 2 % reflectance are used (Labsphere, Sutton, NH). These standards used in the calibration were directly traceable to the US National Institute of Standards and Technology (NIST). For the image intensity of SRS-99 spectralon, we have

$$I_{SRS-99}(x, y, \lambda_k) = L(x, y, \lambda_k)S(x, y, \lambda_k)R_{SRS-99}(\lambda_k) + O(x, y, \lambda_k) \quad (2)$$

And for the image intensity of SRS-02 spectralon, we have

$$I_{SRS-02}(x, y, \lambda_k) = L(x, y, \lambda_k)S(x, y, \lambda_k)R_{SRS-02}(\lambda_k) + O(x, y, \lambda_k) \quad (3)$$

where $R_{SRS-99}(\lambda_k)$ and $R_{SRS-02}(\lambda_k)$ are reflectance functions for these two images and theoretically independent of (x, y) because the spectralon surface has the same reflectance property for all image pixels. By using the equations for $I_{SRS-99}(x, y, \lambda_k)$ and $I_{SRS-02}(x, y, \lambda_k)$, we can derive

$$L(x, y, \lambda_k)S(x, y, \lambda_k) = \frac{I_{SRS-02}(x, y, \lambda_k) - I_{SRS-99}(x, y, \lambda_k)}{R_{SRS-02}(\lambda_k) - R_{SRS-99}(\lambda_k)} \quad (4)$$

10 different spectralon images were obtained and averaged to estimate $I_{SRS-99}(u, v, \lambda)$ and $I_{SRS-02}(u, v, \lambda)$.

With this estimates, the final reflectance is given as below:

$$R(x, y, \lambda_k) = \frac{(I(x, y, \lambda_k) - I_{SRS-99}(x, y, \lambda_k))R_{SRS-02}(\lambda_k)}{I_{SRS-02}(x, y, \lambda_k) - I_{SRS-99}(x, y, \lambda_k)} + \frac{(I_{SRS-02}(x, y, \lambda_k) - I(x, y, \lambda_k))R_{SRS-99}(\lambda_k)}{I_{SRS-02}(x, y, \lambda_k) - I_{SRS-99}(x, y, \lambda_k)} \quad (5)$$

Finally the reflectance $R(x, y, \lambda_k)$ of samples are converted to the apparent absorbance, $A(x, y, \lambda_k)$, defines as the logarithm of the ratio between reflectance of the sample $R(x, y, \lambda_k)$, and the reflectance of certified 99 % standard, measured at the wavelength λ_k and the spatial coordinates x, y [2].

$$A(x, y, \lambda_k) = \log \frac{R_{SRS-99}(\lambda_k)}{R(x, y, \lambda_k)} \quad (6)$$

If the interest region is more than one pixel, the apparent absorbance vector of each ROI is averaging over $M + N$ pixels according to

$$A_{ave}(x, y, \lambda_k) = \frac{1}{M + N} \sum_{j=1}^N \sum_{i=1}^M A(x, y, \lambda_k) \quad (7)$$

This calibration step is performed at the beginning of every experiment.

3. IMAGE ACQUISITION AND ANALYSIS

In this section, we discuss the results of our experimental observations. The aim of these experiments is to demonstrate the potential of HIS for the normal tissue characterization and discriminate it from malign tissues.

3.1. Normal Lung Tissue Characterization

For the normal tissue characteristic experiment, a fresh pig's lung is collected from Temple University Hospital (3401 N. Broad Street. Philadelphia, PA 19140) in April 2008. Totally 91 spectral band images, each image of 1392×1040 pixels in size was obtained within 23 seconds. The 500 W QTH is used for illumination. Samples were kept in iced bags to minimize dehydration and then placed in a tray without ice while hyperspectral images are acquired. To demonstrate the capability of HIS to produce spectral contrast between different regions on the normal lung, four ROI was initially identified based on the visual sense and recorded as normal left lung, normal right lung, normal cardiac notch and normal trachea. The ROI is shown in Fig. 5.

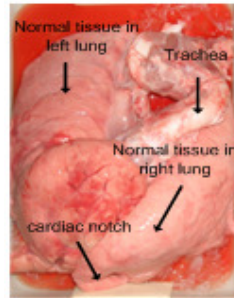


Fig. 5. Four ROI depending on the left lung, right lung, cardiac notch, and trachea.

The primary absorbers of the NIR spectrum in the tissue are deoxyhemoglobin (Hb), oxyhemoglobin (HbO₂), bilirubin and methemoglobin, melanin, and water. Previously reported NIR spectrum characterization of biological tissues show Hb having an absorbance peak at 760 nm, HbO₂ absorbs broadly beyond 800 nm. Bulk lipids have an absorbance peak at 930 nm and water typically peaking at 970 nm [3]. Fig. 6. shows the measured spectrum of ROI of each category. The graph is drawn based on the average of 10×10 pixels apparent absorbance $A(x, y, \lambda_k)$. The range of $A(x, y, \lambda_k)$ is from 0 to 8.307. Within each 10×10 pixels ROI, 100 apparent absorption spectrum of each pixel are calculated and averaged. Since Hb and HbO₂ blood vessels lying over the surface of the lung, a spectrum has a peak of Hb and HbO₂ at 760 nm and 805 nm. The spectrum also indicates significant lipids and water absorption at 905 nm and 970 nm. The wavelength of peak of HbO₂ and bulk lipids we acquired is slightly different from the literature [3]. We expect that this is due to the uncelebrated light source and sample condition. In addition to four peaks, the spectrum has a peak value of 1005 nm, 1035 nm, and 1070 nm due to the mixture of constituents in the lung.

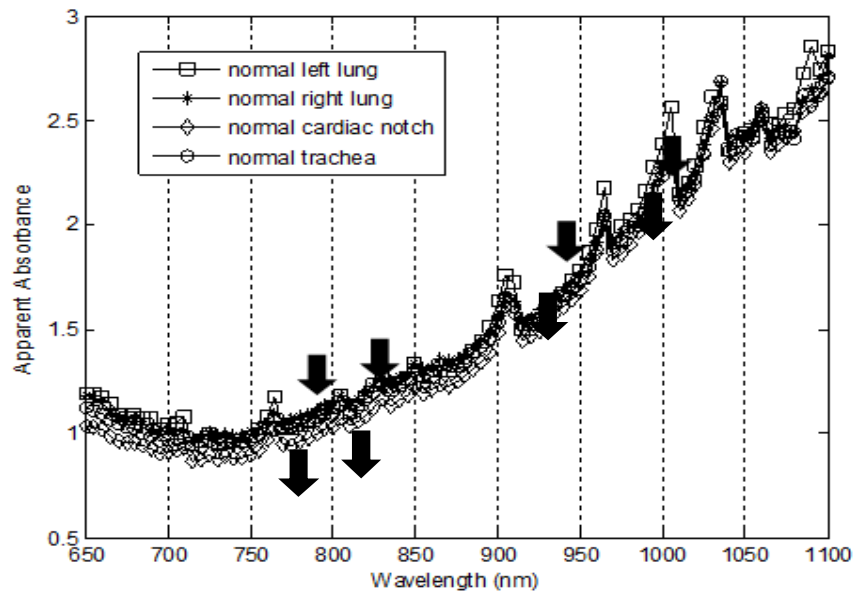


Fig.6. Reconstructed apparent absorbance spectrum of ROI (10×10 pixels) from normal left lung, normal right lung, normal cardiac notch, and normal tracheas. Measured spectra within the area were averaged and plotted. Spectrum contains an absorption peak at 760 nm, characteristic of Hb followed 800 nm peak typical of HbO₂, with lipids at 930 nm and 970 nm for water peak. The peak beyond 970 nm is for a molecular mixture consistent with known constituents contained within lung.

3.2. Simulated Malign Lung Characteristic

For this experiment, the dehydration of lung sample is prepared to mimic unhealthy tissues with regard to reduced scattering, absorption, and autofluorescence. Same as the previous experiment, 91 spectral band images with each image of 1392×1040 pixels in size are obtained. The malign left lung, malign right lung, malign trachea, and malign cardiac notch are determined by 10×10 pixels on each category and 100 apparent absorption spectrum of each pixel are calculated and averaged. Fig. 7. shows the spectrum characteristic of malign lung tissues. It reveals the similar peak of 760 nm, 800 nm, 930 nm 970 nm as normal lung tissues, however the absolute value of apparent absorbance is lower than the normal tissue sample. This is because the malign tissue contains less HbT and water to absorb NIR spectrum. In addition, we notice that from 1050 nm, the spectrum is decreasing whereas the spectrum is still increasing in normal tissue sample.

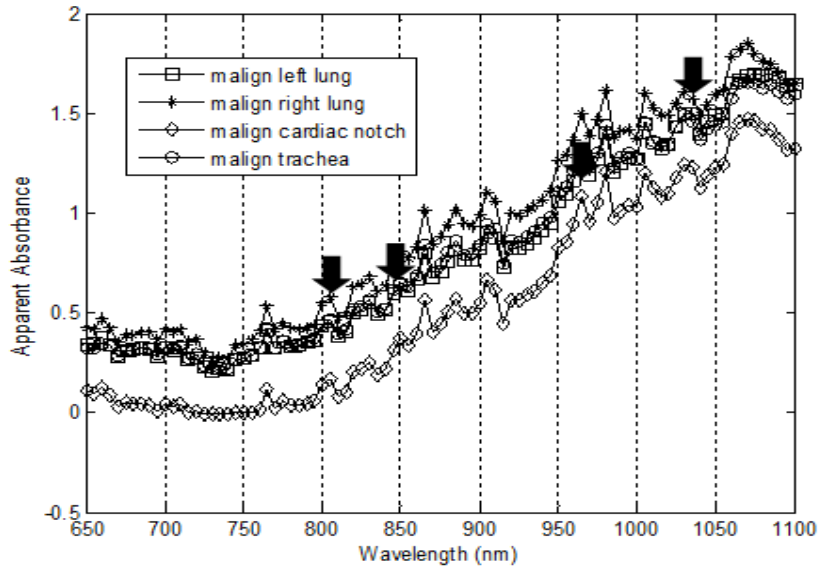


Fig. 7. Reconstructed apparent absorbance spectra of ROI (10×10 pixels) from malign left lung, malign right lung, malign cardiac notch, and malign tracheas. The spectrum has similar peak at 760 nm, 805 nm, 905 nm 970 nm.

3.3. Comparison of Normal and Malign Tissue Characteristics

The complete comparison for the wavelength from 650 nm to 1100 nm, is described in the following discussion. An average intensity value for an area of 10×10 pixels was obtained for normal left lung, normal trachea, malign left lung, and malign trachea. This average absorbance is plotted in Fig. 8. Notice that the major peak in the normal and malignant data occurs at the same wavelength. However, the intensity of malign tissues is significantly less than normal tissues, thus we can easily discriminate between two types of tissues.

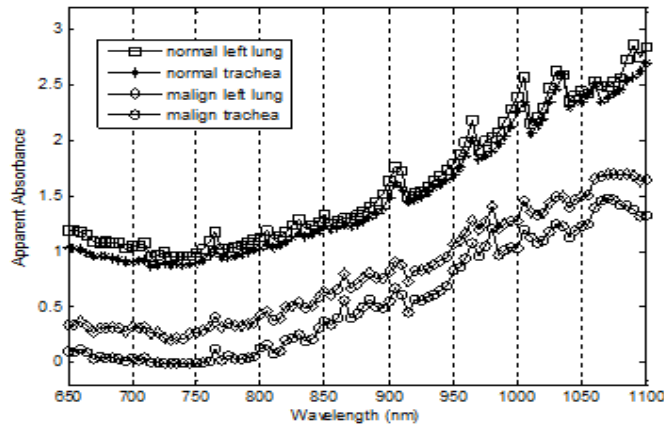


Fig. 8. Comparison of reconstructed apparent absorbance spectra of ROI (10 × 10 pixels) between normal tissue and malign tissues. Two types of tissue has similar wavelength of peak. However the absorbance intensity of malign samples is much lower than normal samples.

It is obvious that an acquisition time of 23s is unacceptable for a clinical instrument, therefore the key wavelength should be chosen. We already find the four key wavelengths of 760 nm, 805 nm, 905 nm, and 970 nm for total hemoglobin, lipids and water. In addition to these wavelengths the ratio between wavelengths are calculated and plotted.

$$r = \lambda_k / \lambda_{k+1}, \quad k = 1, 2, \dots, 90 \tag{8}$$

Since we have totally 91 bands, the number of ratio r would be 8281. Fig. 9. presents the results for the wavelength ratio analysis and Fig. 10. shows the difference of wavelength ratio r between normal and malign tissues. From the results, we notice that when ratio r is 5256, the difference is the biggest. It means the ratio r between 1050 nm and 1100 nm provides the largest difference absorption characteristics between normal and malign tissues. Choosing the key wavelength in this way gives the instrument an acquisition time of approximately one second and differentiates normal and malign tissues simply and effectively.

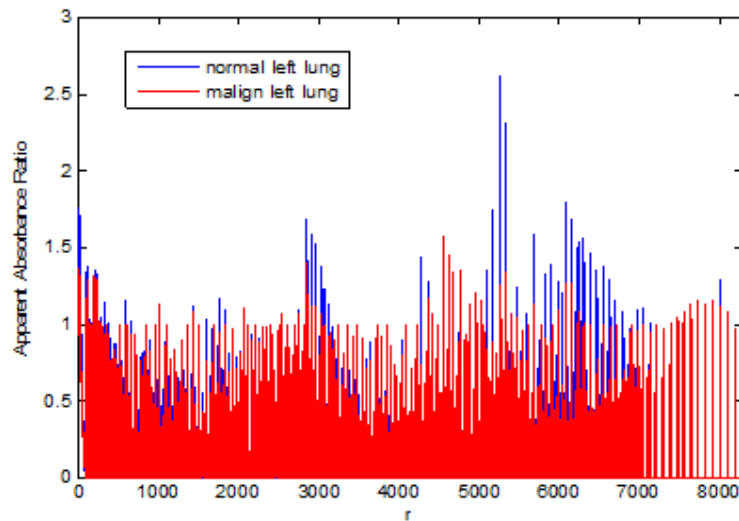


Fig. 9. Wavelength ratio of normal and malign tissues.

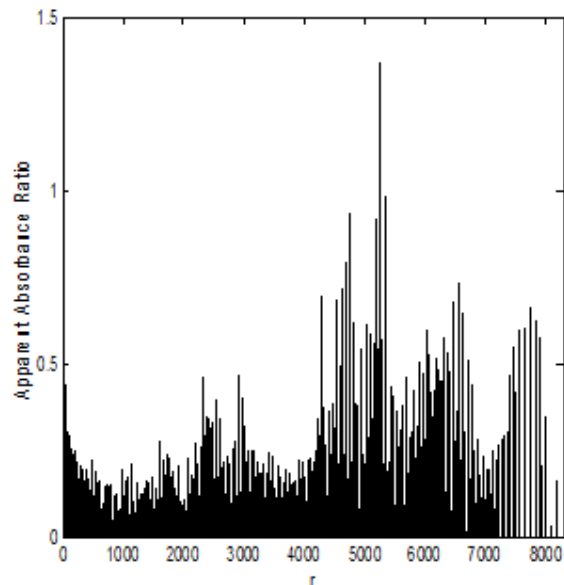


Fig. 10. The difference of wavelength ratio between normal and malignant tissues. We observe that when the ratio is 5256, the difference is the biggest.

4. CONCLUSIONS

In this paper, we describe the development of a hyperspectral imaging system that combines several advances in photonics technologies, including CCD and LCTF. The LCTF is tunable over the spectral range of 650 – 1100 nm. The capability of the system has been proven through phantom lung studies. The apparent absorption differences between normal tissue and malignant tissue have been readily seen using this instrument. Throughout the experiment, we find that NIR imaging technology can provide a new modality for measuring changes in total hemoglobin concentration and oxygenation saturation between normal and malignant human tissue. A key wavelength is also chosen that provides differentiation between normal and malignant samples. This key wavelength reduces the amount of data collected in subsequent work. The system we propose has obvious applications as a medical diagnostic tool. The modality of hyperspectral imaging combined with other data such as CT or MRI may prove useful in the characterization of normal tissues and detection of malignancies.

REFERENCES

- [1] A. Chong, "Digital Near-Infrared Camera for 3D Spatial Data Capture," The 16th Annual Colloquium of the Spatial Information Research Centre, p2004.
- [2] J. Lammertyn, A. Peris, J. Baerdemaeker, and B. Nicolai, "Light Penetration Properties of NIR Radiation in Fruit with respect to Non-destructive Quality Assessment," *Journal of the Postharvest and Technology*, vol. 18, pp. 121-132, Feb. 2000.
- [3] P. Bargo, T. Goodell, R. Steven, GL Kovall, G. Blair, and S. Jacques, "Optical Measurements for Quality Control During Photodynamic Therapy," Plenary Talk Int'l Photodynamic Assoc. Meeting, Jun. 2001.
- [4] P. Bargo, "Optical Measurements for Quality Control in Photodynamic Therapy," Ph. D. Dissertation of Electrical and Computer Engineering, Oregon Health & Science University, Jul. 2003.
- [5] JP. Taroni, A. Pifferi, A. Torricecli, and R. Cubeddu, "Time-Resolved Optical Spectroscopy and Imaging of Breast," *Opto-Electronics Review*, vol. 12, pp. 249-253, 2004.
- [6] Z. Pan, G. Healey, M. Prasad, and B. Trombery, "Face Recognition in Hyperspectral Images," *IEEE Transaction on Pattern Analysis and Machine Intelligence*, vol. 25, no. 12, pp. 1552-1560, 2003.

- [7] K. Zuzak, S. Naik, G. Alexandrakis, D. Hawkins, K. Behbehani, and E. Livingston, "Characterization of a Near Infrared Laparoscopic Hyperspectral Imaging System for Minimally Invasive Surgery," *Analytical Chemistry*, vol. 79, no. 12, pp. 4709-4713, 2007.

ACKNOWLEDGEMENTS

This research was supported by the MOTIE(Ministry of Trade, Industry and Energy), Korea, under the Inter-Economic Regional Cooperation program (R0002625) supervised by the KIAT(Korea Institute for Advancement of Technology) and this work was supported by Business for Cooperative R&D between Industry, Academy, and Research Institute funded Korea Small and Medium Business Administration in 2013

AUTHOR

Jong-Ha Lee

Jong-Ha Lee received the B.S. degree in electronics engineering in 2000 from Inha University, Incheon, Korea, the M.S. degree in electrical engineering in 2005 from Polytechnic Institute of New York University, Brooklyn, NY., and the Ph.D. degree in electrical engineering from Temple University, Philadelphia, PA. He worked at Samsung advanced institute of Technology (SAIT) as a research staff member. Currently, he is an assistant professor with the Department of Biomedical Engineering at Keimyung University, School of Medicine. His current research interests include tactile sensation imaging for tissue characterization, computer-aided diagnosis, medical image analysis, pattern recognition, and machine learning.